Fabrication and Structural Characteristics of Ordered TiO_2−Ru(−RuO_2) Nanorods in Porous Anodic Alumina Films on ITO/Glass Substrate

Song-Zhu Chu,* Kenji Wada, Satoru Inoue, Shun-ichi Hishita, and Keiji Kurashima

Advanced Materials Laboratory, National Institute for Materials Science, Namiki 1-1, Tsukuba, Ibaraki, 305-0044, Japan

Received: May 26, 2003; In Final Form: July 21, 2003

Ordered nanorod (∼ϕ50 nm) arrays of TiO_2−Ru and TiO_2−RuO_2 embedded in porous alumina films were prepared from sputtered Al/ITO films on glass substrates through successive processes of anodization and cathodic electrodeposition. The microstructure of the nanorod arrays was investigated by field-emission scanning electron microscopy and transmission electron microscopy, and the chemical states of the titanium and ruthenium elements in the nanorods were analyzed through X-ray photoelectron spectroscopy. The as-electrodeposited nanorods are composed of ruthenium metal and amorphous titanium(IV) oxide/hydroxide, while the nanorods after being heated at 600 °C for 2 h are polycrystalline and composed of nano-crystals (5−20 nm across) of tetragonal anatase TiO_2 and cubic RuO_2.

1. Introduction

Oxide materials containing titanium and ruthenium are of great interest for their applications in a variety of fields such as photocatalysis, solar cells, electronics, chemical sensors, industrial electrochemistry, and energy storage systems.[1−13] Usually, large surface areas with fine crystal structures (preferably in nanoscale) are required to facilitate ions- and/or electron-transfer reactions. So far, many studies have been devoted to forming various TiO_2−RuO_2, TiO_2, or RuO_2 materials in forms of powders,[1−6] aerogels,[7] and coatings[8−18] by means of sol−gel method,[1−11] sputtering deposition,[12−14] and electrodeposition.[15−18] Especially, electrochemical deposition techniques, which are conventionally used to achieve various metal and alloy coatings on conductive substrates, have attracted much attention for the low cost of equipment and starting materials and for the ability to deposit desired oxides without impurities such as carbon from organic solvents in a sol−gel process.

Cathodic electrodeposition of TiO_2−RuO_2 coatings has been conducted in several studies.[15−18] It is usually considered that the electrodeposition is based on the electrochemical production of OH^- ions from the cathodic reduction of water or dissolved oxygen that promotes the precipitation of oxides and/or hydroxides of metal ions or complexes contained in the electrolytic medium on the cathodic substrate. The solid oxide and/or hydroxide precursors, usually unstable with an amorphous nature, are thermally decomposed at elevated temperatures to obtained stable oxide coatings. Nevertheless, the as-electrodeposited titanium and ruthenium species, which were usually considered as oxides or hydroxides, are actually still not confirmed, because a multistep electrodeposition mode accompanied with preheating was often adopted to acquire thick coatings and the fresh as-electrodeposits could not be investigated. The chemical states and the crystal structures of the electrodeposits are still not fully understood, which are usually essential to elucidate the characteristics for various applications.

The present work aims to explore a new route for fabricating nanostructured TiO_2−RuO_2 materials, i.e., composite TiO_2−Ru(−RuO_2) nanorod arrays directly on ITO/glass by combining aluminum anodization with cathodic electrosynthesis, which are expected to hold some distinctive properties different from conventional coatings for many potential applications. In this paper, we report the preparation of TiO_2−Ru and TiO_2−RuO_2 composite nanorods in nanopores anodic alumina films on ITO/glass through a cathodic electrodeposition followed by a successive calcination. The microstructural characteristics and chemical-state transition of electrodeposited TiO_2−Ru(−RuO_2) nanorods on ITO/glass are investigated by field-emission scanning microscopy (FESEM), transmission electron microscopy (TEM), energy-dispersive X-ray analysis (EDX), and X-ray photoelectron spectroscopy (XPS).

2. Experimental Section

2.1. Specimens. Highly pure aluminum film (99.99%, ∼1.5 μm) was deposited on a soda-lime glass (25 × 110 × 0.7 mm) covered with a tin-doped indium oxide (ITO: ∼120 nm, ∼10 Ω/□) film through a RF-sputtering at a rate of 1.5 nm/s. Other conditions on sputtering deposition are the same as in previous studies.[19,20] Here, the ITO film is adopted to ensure the complete anodization of aluminum layer and used as a transparent conductive layer in cathodic electrodeposition.

2.2. Anodization. After being degreased by acetone in an ultrasonic bath for 10 min, the specimens were anodically oxidized in a 3 wt % oxalic acid solution at 40 V and 10 °C, until all the Al layer was anodized into the oxide, featured by a gradual change into a transparent one. Prior to cathodic electrodeposition, the anodized specimens were immersed in a 5 vol % phosphoric acid solution at 30 °C for 15 min, to remove the insulative barrier layer of anodic alumina films and expose the conductive underlying ITO film to the electrolyte.

2.3. Electrodeposition. The electrolyte was a mixed ethanol−water (3:1 in volume ratio) solution containing titanium chloride (0.02 M $TiCl_3$), ruthenium chloride (800 ppm $RuCl_3 \cdot nH_2O$), and peroxide (0.08 M H_2O_2, 30% in water). Cathodic elec-

* Author to whom correspondence should be addressed. Phone: +81 29 851 3354 (ext 8600). Fax: +81 29 854 9060. E-mail: CHU.Songzhu@nims.go.jp.

10.1021/jp0354503 CCC: $25.00
Published on Web 08/26/2003

trosynthesis was performed at a constant current density of 100 A/m^2 (net current density) and 1 °C, with vigorous stirring. The operating current density, i.e., the overall current density that related to the apparent surface area of the specimen, was determined by calculating the porosity of the anodic alumina films, as described later. A platinum plate (99.98%, 30 × 150 × 2 mm) was used as the counter electrode. The distance between the specimens and the platinum electrode is set to be ~2 cm. The electrodeposition was continuously carried out for 4−10 min, till the specimens changed from a transparent into an opaque one. After drying at room temperature in the air, the as-electrodeposited specimens were heated at 600 °C for 2 h at a rate of 2 °C/min to fulfill crystallization.

2.4. Characterizations. The morphology of the specimens was observed by a field emission scanning electron microscope (FESEM: S-5000, Hitachi) with an energy-dispersive X-ray analyzer (EDX) after osmium evaporation. The X-ray photoelectron spectroscopy analysis (XPS) was performed by a 5 channeltron analyzer (VG Scientific ESCALAB 200-X) under an operating vacuum better than 1×10^{-9} Torr using the Mg Kα ray. Before analysis, the specimens were sputter-cleaned for 10 min to eliminate the oxide film on the surface of the deposits. The binding energy of the spectra was corrected by the O1s signal, assumed to be 531.0 eV. The binding energy was accurate to within 0.1 eV. The crystallographic structures of the specimens were observed by transmission electron microscopes (TEM: JEOL-200 kV for heated samples and JEOL-300 kV for as-deposited samples). The composite layers were first scratched off from ITO/glass substrates and smashed and then set on carbon-coated copper micro-grids for TEM observation.

3. Results and Discussion

3.1. Microstructures of Porous Alumina Films on ITO/Glass. Formation of an anodic alumina film with a uniform porous structure on the ITO/glass substrate is an important prerequisite, since the successive electrodeposited nanorods will inherit the geometrical shape of the alumina template. Figure 1 shows the FESEM images of the fracture section and surface morphology of the specimens anodized down to the ITO/glass substrate. The anodic alumina film comprises uniform and periodic nanopores with 30 nm in diameters and 100 nm in pore interspacing and ordered parallel channels perpendicular to the substrates.

Especially, from the high-resolution images (insert in Figure 1a), the resultant anodic alumina film possesses an abnormal thin barrier layer that is approximately only one-fifth of the pore walls (see arrows). This characteristic thin barrier layer may be ascribed to the local chemical dissolution of the barrier layer at the Al−ITO interface near the ending of anodization, which is enhanced by the local increases of temperature (electrode transition from aluminum to ITO film) and/or acidity (electrolysis of water).[20] The characteristic thin barrier layer of anodic alumina films on ITO/glass enables the removal of the insulative alumina barrier layer through appropriate chemical dissolution without damaging the geometric shape of alumina nanostructure and the exposure of the underlying conductive ITO film to the electrolyte.

Figure 1b shows the surface morphology of the porous anodic alumina films after removing the barrier layer by a chemical dissolution. The pore distribution is uniform and the average pore size is ~50 nm in diameter. The ordering of the nanopores, when necessary, can be improved through a pre-texturing procedure like pre-indentation.[21,22] According to calculation, the pore density and the porosity of the alumina film shown in Figure 1b are approximately 4.2×10^{14} ($pore/m^2$) and 0.38, respectively.

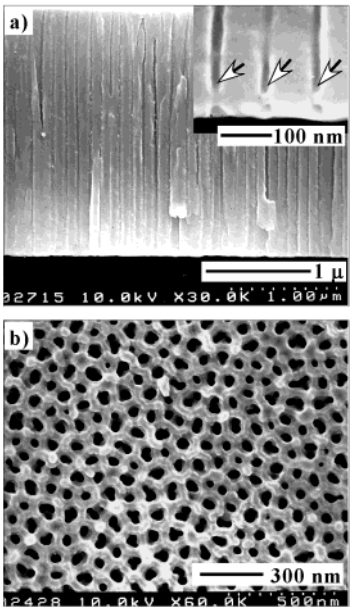

Figure 1. FESEM images of (a) vertical fracture section and (b) surface morphology of porous alumina films anodized down to the ITO/glass substrate in a 3% oxalic acid solution at 40 V and 10 °C. Before imaging (b), the specimen was immersed in 5% H_3PO_4 solution at 30 °C for 15 min. Insert in (a) is a high-resolution image near the barrier layer of the alumina film.

3.2. Fabrication of $TiO_2-Ru(-RuO_2)/Al_2O_3$ Composite Nanostructures on ITO/Glass. The porous alumina nanostructure on ITO/glass after removing the barrier layer was used as the template electrode in cathodic electrodeposition in an electrolyte containing titanium and ruthenium ions. To maintain a net current density of 100 A/m^2 (corresponding to the exposed ITO area in alumina films), the overall current density (corresponding to appearance area of the specimen) was set at 38 A/m^2, on the basis of the porosity (0.38) of the alumina films calculated before. At the beginning of the electrodeposition, the transparent template electrode with porous alumina films became nearly uniformly black, indicating the filling of the electrodeposits into the pores of the alumina film. The operating voltage between the electrodes was always increasing during the electrodeposition, first quickly and then slowly after a few seconds. The operating voltage even reached more than 50 V at the last stage, inferring the low conductive nature of the electrodeposits. To achieve complete filling in the nanopores, the deposition went on until the black deposits formed a continuous film on the electrode. In the case of overfilling, the as-electrodeposited coating was bright black with metallic luster when fresh and wet, but lost the luster and became translucent after drying in the air for a few minutes, possibly due to the dehydration and/or the oxidation on the surface of electrodeposits in the air. After being heated at 600 °C for 2 h, the specimens become transparent with a slight gray color, inferring the oxidation of the electrodeposits.

3.3. Microstructures of $TiO_2-Ru(-RuO_2)/Al_2O_3$ Composite Nanostructures. Figure 2 shows the FESEM images of the fracture sections of the electrodeposited specimens before and after heating. The electrodeposits (TiO_2-Ru or TiO_2-RuO_2, see EDX and XPS analysis later) are filled in the pores of alumina films uniformly and densely (Figures 2a and 2c) and form a continuous layer on the top of alumina films (Figure 2b). The as-electrodeposited nanorods (Figure 2a) show a

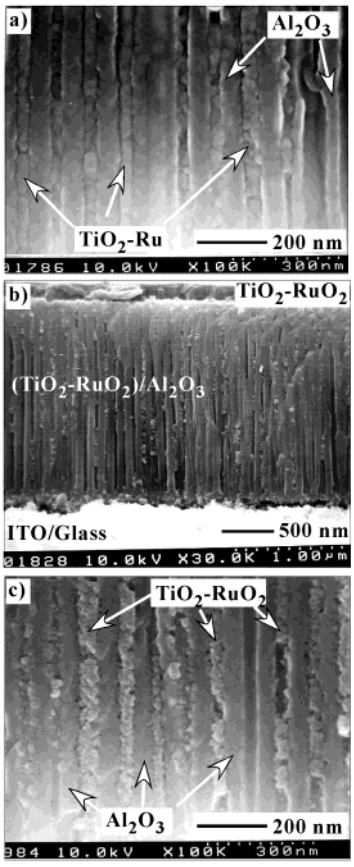

Figure 2. FESEM images of the vertical fracture sections for various composite nanorods embedded in porous alumina films on ITO/glass substrates: (a) as-electrodeposited specimen, and (b) & (c) after heating at 600 °C for 2 h.

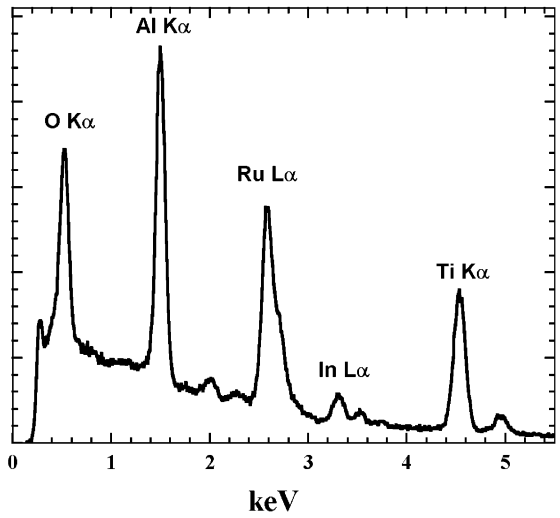

Figure 3. A typical EDX spectrum for an as-electrodeposited specimen.

smooth surface with fine appearance, while the sintered nanorods (Figure 2c) exhibit a granular structure containing tiny grains and many voids, inferring the oxidation and crystallization. On the basis of the thickness of porous alumina films (~2.2 μm), the aspect ratio of the nanorods (~50 nm) is estimated to be 44.

Figure 3 displays a typical EDX spectrum for the as-electrodeposited specimen. Besides Al Kα, O Kα, and In Lα, which can be ascribed to the alumina film and the underlying ITO film, a Ti Kα peak and a Ru Lα peak appear in the spectrum, indicating that the electrodeposits contain titanium

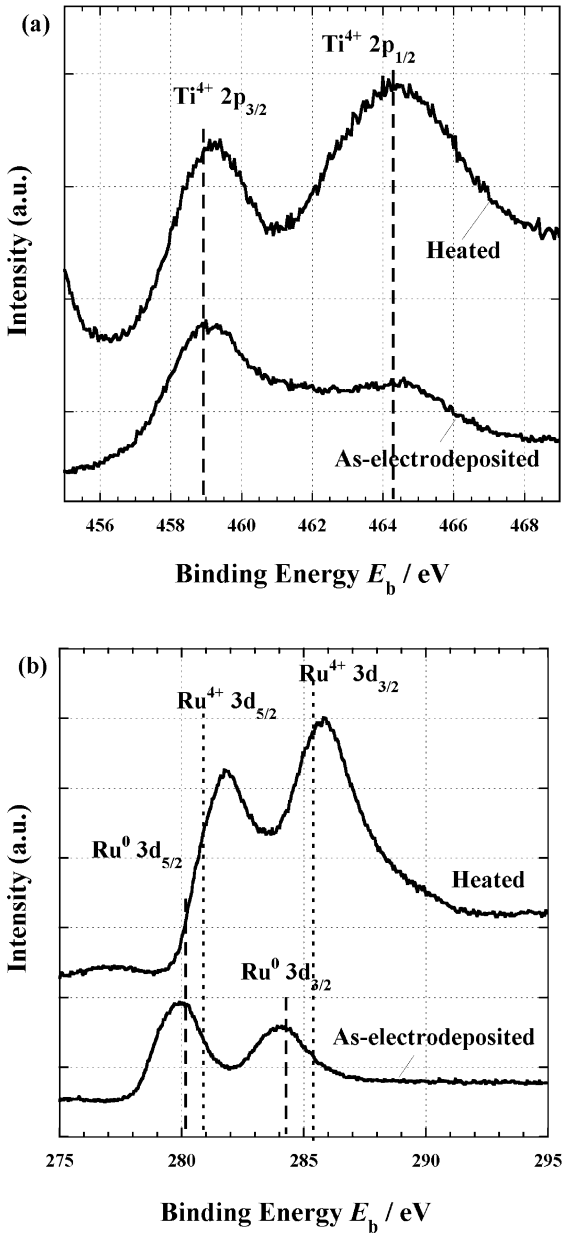

Figure 4. High-resolution XPS spectra of (a) Ti 2p and (b) Ru 3d for electrodeposited specimens before and after heating.

and ruthenium elements. The atomic ratio of titanium to ruthenium in the electrodeposits is estimated to be 70:30. In addition, it is also found in preliminary experiments that the ruthenium content in the electrodeposits changes proportionally with the current density, indicating that the compositions of the electrodeposits can be simply controlled by adjusting the current density as conventional alloy electrodeposition.

3.4. Chemical States of Titanium and Ruthenium. Usually, electrodeposition of transition metals (Ti, Zr, Nb, Ru, etc.)[15−18] may yield hydroxides/oxides or metals, or both simultaneously. To investigate the chemical state of titanium and ruthenium elements in the electrodeposits, XPS measurements were carried out on the electrodeposited specimens before and after heating. The high-resolution XPS spectra of Ti 2p and Ru 3d for as-electrodeposited and heated specimens are shown in Figure 4. For the as-electrodeposited specimen, the binding energies of the Ti 2p spectrum (Figure 4a) are 459.0 eV ($2p_{3/2}$) and 464.5 eV ($2p_{1/2}$), which are close to the binding energies of a standard TiO_2 spectrum at 458.8 eV ($2p_{3/2}$) and 464.3 eV ($2p_{1/2}$) (see

broken lines), indicating that the titanium in the as-electrodeposits exists in the Ti(IV) oxidation state as peroxides and/or hydroxides. Whereas for the Ru 3d spectrum of the as-electrodeposited specimen (Figure 4b), two peaks appear at the binding energies of 279.8 eV−$3d_{5/2}$) and 284 eV−$3d_{3/2}$), which are slightly lower than those of the metallic ruthenium situated at 280.1 eV−$3d_{5/2}$ and 284.2 eV−$3d_{3/2}$ (see broken lines). This strongly suggests that the ruthenium metal is formed in electrodeposition through a redox reaction in the cathodic electrodeposition. Moreover, from the narrow fwhm (2.37 eV−$3d_{5/2}$), it can be deduced that ruthenium in the as-electrodeposits exists in a single chemical state, i.e., metal state. The metallic ruthenium in the electrodeposits may work as a conductive component to allow the continuous electrodeposition for a certain period. In addition, on the basis of the integral areas of the Ti 2p and Ru 3d peaks, the atomic ratio of Ti to Ru was calculated to be 69:31 (or TiO_2−32 at. % Ru), which agrees well with the result of the EDX analysis.

The XPS spectra of Ti 2p and Ru 3d for the specimen after heating at 600 °C for 2 h are also shown in Figure 4. The binding energies of Ti 2p for the heated sample are also close to those of the Ti(IV) oxidation state but have shifted ∼0.3 eV to the right compared to the as-electrodeposited sample, inferring that titanium exists in a Ti(IV) oxide state but with a relatively stable structure, i.e., crystallized structure as described later. While for the Ru 3d spectrum, the binding energies have shifted to 281.8 eV ($3d_{5/2}$) and 285.9 eV ($3d_{3/2}$), which are apparently higher than those of standard Ru(IV) oxide at 280.8 eV ($3d_{5/2}$) and 285.0 eV ($3d_{3/2}$) (see dotted lines). This strongly suggests that the metallic ruthenium in electrodeposits has been completely transferred to ruthenium(IV) oxide during the heat treatment.

3.5. Crystallographic Structures of $TiO_2-Ru(-RuO_2)$ Nanorods. The crystallographic structures of the composite nanomaterials are very important in explaining the characteristics for various applications. It was found in XRD analysis (not shown) that only broad humps appeared in the patterns for both as-electrodeposited and heated specimens, possibly due to the amorphous or fine crystal structures and the thin thickness of the composite layers. Therefore, transmission electron microscopy was used to investigate the crystal structures of the electrodeposits with and without heating, which is first reported by the present study. Figure 5 shows a TEM image of a bundle of free nanorods and the corresponding diffraction pattern for an as-electrodeposited specimen. The nanorods under the TEM seem not as dense and uniform as the FESEM image (Figure 2a). Some voids can be observed in the nanorods. In fact, the voids were mostly generated under the irradiation of the electron beam (300 kV) during the TEM observation, indicating the unstable nature of the as-electrodeposits. The voids may be caused by dehydration and/or the decomposition of the titanium-electrodeposits that may exist in hydroxides or peroxides. The corresponding electron diffraction pattern (Figure 5b) exhibits several continuous reflections which are all indexed to ruthenium metal. This also confirmed the existence of ruthenium in the as-deposited nanorods, consistent with the result of XPS analysis (Figure 4). In addition, there is no reflection corresponding to crystallized titanium oxide in the diffraction pattern, suggesting an amorphous structure.

Figure 6a shows a TEM image of TiO_2-RuO_2/Al_2O_3 composite layer after heated at 600 °C for 2 h. Numerous tiny grains ranging from 5 to 20 nm can be observed inside the pores of alumina films, though some of the grains have come out from the pores during the preparation of the sample. The selected

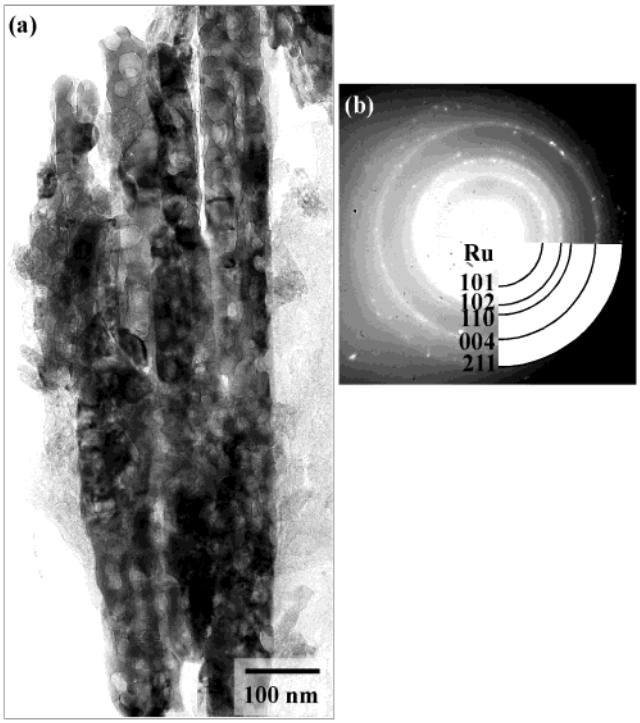

Figure 5. (a) TEM image of a bundle of free TiO_2-Ru nanorods from an as-electrodeposited specimen, (b) the corresponding electron diffraction pattern of the nanorods.

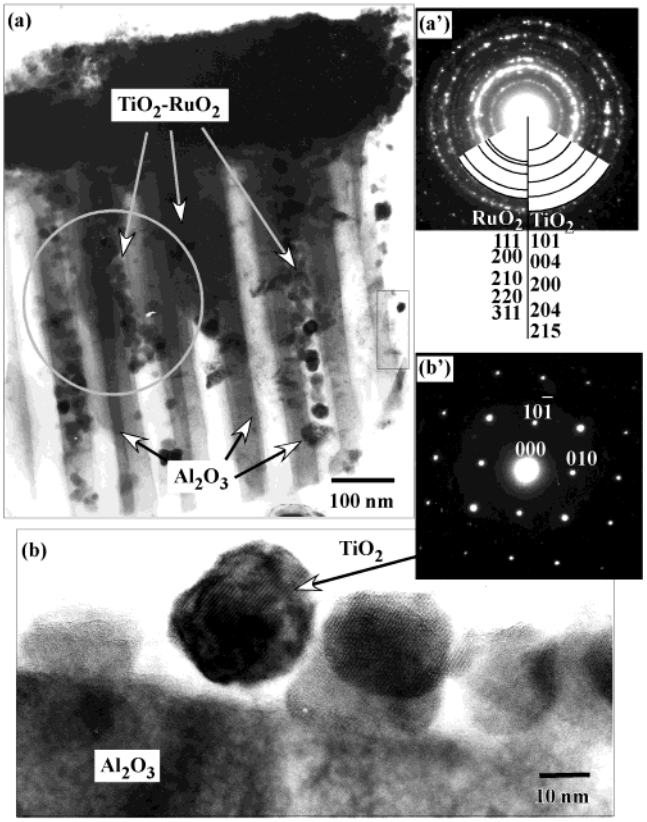

Figure 6. (a) Low- and (b) high-resolution TEM images of TiO_2-RuO_2/Al_2O_3 composite layer heated at 600 °C for 2 h. (a′) and (b′) are the selected area electron diffraction patterns corresponding to the circled area in (a) and a grain in (b), respectively.

area electron diffraction pattern (6a′) corresponding to the circled area shows several strong and discontinuous reflections, suggesting a polycrystalline structure. It was found that the blank anodic alumina after heating exhibited a hollow electron

diffraction pattern (not shown), indicating that alumina still remains amorphous under 600 °C. Thus, all the rings in Figure 6a′ are ascribed to the heated electrodeposits. According to calculation, the reflections, as indicated in the pattern, correspond closely to those of tetragonal anatase TiO_2 with the lattice constants $a = 3.7852$ Å and $c = 9.5139$ Å (Card No.21-1272) and those of cubic RuO_2 with the lattice constants $a = 4.85892$ Å (Card No.87-0726), confirming the crystallization of TiO_2 and RuO_2. A HRTEM image of the composite layer (Figure 6b) accompanied with a characteristic single-crystalline diffraction pattern (Figure 6b′) suggests that the TiO_2-RuO_2 composite nanorods are composed of numerous single crystals. The selected area electron diffraction pattern is also indexed to a tetragonal anatase TiO_2 single crystal as described above. In addition, RuO_2 in single crystals was not detected in the HRTEM image, possibly due to the very small sizes of RuO_2 grains which may be originally embedded in the grain boundaries of relatively large TiO_2 grains but exfoliated away during the preparation of the sample.

4. Conclusions

We fabricated successfully TiO_2-Ru and TiO_2-RuO_2 nanorods ($\sim\phi$50 nm) in porous anodic alumina films on ITO/glass through successive anodization and cathodic electrodeposition. The cathodic electrodeposition through the porous anodic alumina template yields a composite TiO_2-Ru, and the sintering at appropriate temperature produces a nano-crystalline TiO_2-RuO_2. The TiO_2-Ru and TiO_2-RuO_2 nanorod arrays on ITO/glass, when released from alumina templates by a selective etching,[23] can be used for many potential applications such as photocatalysis, photocells, and photoelectrochemical investigations. It has been confirmed that the integrated TiO_2-RuO_2 nanorods exhibit higher photocatalytic activity than the conventional flat TiO_2 film because of their large surface area and effective contact to the reactant substances. Moreover, the present approach can be applied to fabricate other metal/oxide composite nanostructures from transition metals such as Zr, Nb, Ta, and typical metals such as Pb, Pt, and Pd for dielectric and/or catalytic applications, which are being explored.

Acknowledgment. This work is supported by the Japanese Millennium Project of "Exploration and Creation of a Catalyst for Removing Harmful Chemical Substances".

References and Notes

(1) Kawai, T.; Sakada, T. *Chem. Phys. Lett.* **1980**, *72* (1), 87.

(2) Zheng, J. P.; Cygan, P. J.; Jow, T. R. *J. Eletrochem. Soc.* **1995**, *142* (8), 2699.

(3) van Zyl, W. E.; Winnubst, L.; Raming, T. P.; Schmuhl, R.; Verweij, H. *J. Mater. Chem.* **2002**, *12*, 708.

(4) Miller, J. M.; Dunn, B.; Tran, T. D.; Pekala, R. W. *J. Eletrochem. Soc.* **1997**, *144* (12), L309.

(5) Nanaumi, T.; Ohsawa, Y.; Kobayakawa, K.; Sato, Y. *Electrochemistry* **2002**, *70* (9), 681.

(6) Kameyama, K.; Tsukada, K.; Yahikozawa, K.; Takasu, Y. *J. Eletrochem. Soc.* **1993**, *140* (4), 966.

(7) Swider, K. E.; Merzbacher, C. I.; Hagans, P. L.; Rolison, D. R. *Chem. Mater.* **1997**, *9*, 1248.

(8) Guglielmi, M.; Colombo, P.; Rigato, V.; Battaglin, G.; Boscolo-Boscoletto, A.; DeBattisti, A. *J. Eletrochem. Soc.* **1992**, *139* (6), 1655.

(9) Cornell, A.; Simonsson, D. *J. Eletrochem. Soc.* **1993**, *140* (12), 3123.

(10) Vadimsky, R. G.; Frankenthal, R. P.; Thompton, D. E. *J. Eletrochem. Soc.* **1979**, *126* (11), 2017.

(11) Hine, F.; Yasuda, M.; Yosida, T. *J. Eletrochem. Soc.* **1977**, *124* (4), 500.

(12) Green, M. L.; Gross, M. E.; Papa, L. E.; Schnoes, K. J.; Brasen, D. *J. Eletrochem. Soc.* **1985**, *132* (11), 2677.

(13) Vijay, D. P.; Desu, S. B. *J. Eletrochem. Soc.* **1993**, *140* (9), 2640.

(14) Kim, H. K,; Seong, T. Y.; Lim, J. H.; Ok, Y. W.; Cho, W. I.; Shin, Y. H.; Yoon, Y. S. *J. Vac. Sci. Technol. B* **2002**, *20* (5), 1827.

(15) Zhitomirsky, I. *J. Mater. Sci.* **1999**, *34*, 2441.

(16) Zhitomirsky, I. *Mater. Lett.* **1998**, *33*, 305.

(17) Zhitomirsky, I. *J. Eur. Ceram. Soc.* **1999**, *19*, 2581.

(18) Peiró, A. M.; Brillas, E.; Peral, J.; Domènech, X.; Ayllón, J. A. *J. Mater. Res.* **2002**, *12*, 2769.

(19) Chu, S. Z.; Wada, K.; Inoue, S.; Todoroki, S. *J. Electrochem. Soc.* **2002**, *149* (7), B321.

(20) Chu, S. Z.; Wada, K.; Inoue, S.; Todoroki, S.; Takahashi, Y. K.; Hono, K. *Chem. Mater.* **2002**, *14* (11), 4595.

(21) Masuda, H.; Fukuda, K. *Science* **1995**, *268*, 1466.

(22) Masuda, H.; Yanagishita, T.; Yasui, K.; Nishio, K.; Yagi, I.; Rao, T. N.; Fujishima, A. *Adv. Mater.* **2001**, *13* (4), 247.

(23) Chu, S. Z.; Wada, K.; Inoue, S. *Adv. Mater.* **2002**, *14* (23), 1752.